

# Airborne lidar reflectance measurements at $1.57\ \mu\text{m}$ in support of the A-SCOPE mission for atmospheric $\text{CO}_2$

A. Amediek<sup>1</sup>, A. Fix<sup>1</sup>, G. Ehret<sup>1</sup>, J. Caron<sup>2,\*</sup>, and Y. Durand<sup>2</sup>

<sup>1</sup>Deutsches Zentrum für Luft- und Raumfahrt (DLR) Oberpfaffenhofen, Institut für Physik der Atmosphäre, 82234 Wessling, Germany

<sup>2</sup>ESA/ESTEC, Earth Observation Project Department, 2201 AZ Noordwijk, The Netherlands

\* working as consultant from RHEA System SA

Received: 2 June 2009 – Published in Atmos. Meas. Tech. Discuss.: 24 June 2009

Revised: 29 October 2009 – Accepted: 5 November 2009 – Published: 26 November 2009

**Abstract.** The characteristics of the lidar reflectance of the Earth's surface is an important issue for the IPDA lidar technique (integrated path differential absorption lidar) which is the proposed method for the spaceborne measurement of atmospheric carbon dioxide within the framework of ESA's A-SCOPE project. Both, the absolute reflectance of the ground and its variations have an impact on the measurement sensitivity. The first aspect influences the instrument's signal to noise ratio, the second one can lead to retrieval errors, if the ground reflectance changes are strong on small scales. The investigation of the latter is the main purpose of this study. Airborne measurements of the lidar ground reflectance at  $1.57\ \mu\text{m}$  wavelength were performed in Central and Western Europe, including many typical land surface coverages as well as the open sea. The analyses of the data show, that the lidar ground reflectance is highly variable on a wide range of spatial scales. However, by means of the assumption of laser footprints in the order of several tens of meters, as planned for spaceborne systems, and by means of an averaging of the data it was shown, that this specific retrieval error is well below 1 ppm ( $\text{CO}_2$  column mixing ratio), and so compatible with the sensitivity requirements of spaceborne  $\text{CO}_2$  measurements. Several approaches for upscaling the data in terms of the consideration of larger laser footprints, compared to the one used here, are shown and discussed. Furthermore, the collected data are compared to MODIS ground reflectance data.

## 1 Introduction

A-SCOPE (Advanced Space Carbon and Climate Observation of Planet Earth) is one of the six candidate Earth Explorer missions which have been selected by the European Space Agency (ESA) for assessment studies (ESA, 2008). This mission aims at the determination of regional sources and sinks of  $\text{CO}_2$  by means of inverse modeling using global observations of  $X\text{CO}_2$  (column-weighted dry-air mixing ratio of atmospheric  $\text{CO}_2$ ) in the near infrared spectral region (ESA, 2008). A-SCOPE will have its own light source emitting pulsed narrow-line laser radiation either in the  $1.6\ \mu\text{m}$  or  $2.0\ \mu\text{m}$  spectral range. It will use a range-gated receiver for distinguishing between the signals backscattered from the Earth surface, clouds or elevated aerosol layers. The retrieval of  $X\text{CO}_2$  is based on the Integrated Path Differential Absorption (IPDA) lidar method which allows to measure the  $\text{CO}_2$  Differential Atmospheric Optical Depth (DAOD) from top of the atmosphere down to the Earth's surface by comparing the lidar echoes at two transmitted wavelengths (termed as on- and off-line) in the vicinity of the selected  $\text{CO}_2$ -absorption line (Ehret et al., 2008).

The random error characteristics of the measured DAOD and hence the quality of the retrieved  $X\text{CO}_2$  values from A-SCOPE observations strongly depends on the type of surface. The surface reflectance characteristics are quite different for land and water. In general the reflectivity of the sea is caused by specular reflection on the water surface, by backscattering due to whitecaps, and by subsurface backscattering (Menzies et al., 1998). As well-known from previous studies, over the ocean the lidar reflectance will strongly be anticorrelated to the surface wind speed which effects the possibility for



Correspondence to: A. Amediek  
(axel.amediek@dlr.de)

specular reflectance leading to strong lidar echoes (Cox and Munk, 1954; Bufton et al., 1983). This is due to the slope probability distribution of sea waves which results in a higher reflectivity in case of low wind speeds and vice versa (Cox and Munk, 1954). Due to the small penetration depth in water for wavelengths in the near IR around 1.6  $\mu\text{m}$ , the magnitude of the diffuse (non-directional) scattering component on water particles is expected to be negligible compared to the glint (directional) reflectance given for the typical lidar geometry (Friedman, 1969). In contrast to the ocean, land surfaces usually provide higher reflectance values, although the directional characteristic (e.g. hot spot over vegetation) is less pronounced (Baldrige et al., 2009; Bréon et al., 2002). However, the brightness of the various surface types can vary substantially for different wavelengths as shown for example by the results from 1.6  $\mu\text{m}$  channel of the MODIS (Moderate Resolution Imaging Spectroradiometer) instrument (Justice et al., 2002). The resulting reflectivity gradient associated to a particular reflectance pattern is assumed to provide an additional source of error if the footprints from on- and offline laser pulses do not spot on the same target on ground (Ehret et al., 2008). Such footprint shifts may occur either from misalignment of the transmitted laser beams (e.g. laser pointing jitter) or from the finite time separation between the online and offline pulses. This separation is required, because the detector system does not select the individual wavelengths and thus a temporal overlap between a ground signal from the first pulse with a signal coming from upper tropospheric layers of the subsequent pulse has to be avoided. Due to the satellite velocity (close to 7000 m/s for low-altitude orbits), the time delay (typically larger than 200 microseconds) creates a spatial shift of a few meters between the areas illuminated by the laser pulses on ground.

To analyse the particular error contribution and to setup an optimum sensor design for the A-SCOPE mission a better data basis on the relevant surface reflectance as well as its variability in the spectral domain around 1.57  $\mu\text{m}$  is of outmost interest. Airborne measurements are suited for such kind of investigation because of the similar viewing geometry as provided by the spaceborne counter part. The small footprint on ground of a few meters in diameter allows to investigate the reflectance statistics over complex terrain with high spatial resolution. For the footprint size of the spaceborne sensor, which is in the order of 100 m, representative values (e.g. mean and variance) can be obtained from upscaling of the airborne measurements. The high flexibility of the aircraft platform allows for remote measurements at almost all geographical locations around the world. Particularly in Europe, strong gradients in the surface reflectivity are expected over areas with heavy land use (large agriculture areas with patches of forest and meadows) and snow cover combined with vegetation and wooded terrain, whereas measurements in winter and summer time would enable to observe seasonal trends.

In this study we investigate the surface reflectance at 1.57  $\mu\text{m}$  using an airborne platform covering different terrains in Central and Western Europe as well as the Baltic and Mediterranean Sea. The system is optimized to avoid an interference due to  $\text{CO}_2$  or  $\text{H}_2\text{O}$  absorptions. So, only the ground reflectivity signature is captured, and the focus is put on its small scale variations. Section 2 describes the calculation of the retrieval error and different laser footprint upscaling approaches to establish a connection to spaceborne systems. In Sect. 3 the experimental setup and the measured data are described. Section 4 gives an overview of the collected data. In Sect. 5 the comparison of the collected data with absolute reflectances from satellite measurements is shown and a calibration using these data is discussed. Section 6 shows a comparison and discussion of the different upscaling approaches. Section 7 summarizes the results of statistical analyses. In Sect. 8 the retrieval error simulation results for the A-SCOPE system configuration on the basis of the collected data are presented.

## 2 Theory

### 2.1 Calculation of the retrieval error

The retrieval error of a trace gas IPDA measurement introduced by ground reflectance variations is derived from the hard target lidar equation (Ehret et al., 2008). For a lidar system the detected power  $P$  of the ground return can be expressed as

$$P = \rho S e^{-2\tau} \quad (1)$$

with the lidar ground reflectance  $\rho$  (in  $\text{sr}^{-1}$ ),  $S$  as the instrument constant and  $\tau$  as the measured optical depth.

In the case of a differential absorption measurement, like IPDA,  $P_{\text{on}}/P_{\text{off}}$  is calculated. That leads to the trace gas differential optical depth  $\Delta\tau_{\text{gas}} = \tau_{\text{on}} - \tau_{\text{off}}$  that is equal to

$$\Delta\tau_{\text{gas}} = \frac{1}{2} \left( \ln \frac{P_{\text{off}}}{P_{\text{on}}} + C \right) \quad (2)$$

For an ideal measurement the system constant cancels out, but  $C = \ln(\rho_{\text{on}}/\rho_{\text{off}})$  remains, if the reflectances are not equal for online and offline.

The data obtained by a spaceborne IPDA lidar system are intended for the determination of the column weighted volume mixing ratio of a trace gas which is defined as (Ehret et al., 2008)

$$X_{\text{gas}} = \frac{\Delta\tau_{\text{gas}}}{\int_{\text{Gnd}}^{\text{TOA}} w(p, T) dp} \quad (3)$$

with the weighting function  $w(p, T) = n_{\text{air}}(p, T) \cdot (\sigma_{\text{on}}(p, T) - \sigma_{\text{off}}(p, T)) \cdot (-\partial r / \partial p)$ , integrated from the ground to the top of the atmosphere ( $n_{\text{air}}$  represents the number density of the air,  $\sigma$  the trace gas absorption cross

section, both given in pressure  $p$  and temperature  $T$  coordinates). The relative error of  $X_{\text{gas}}$ , if  $\rho_{\text{on}} \neq \rho_{\text{off}}$ , turns out to be

$$\frac{\delta X_{\text{gas}}}{X_{\text{gas}}} = \frac{1}{2 \Delta \tau_{\text{gas}}} \ln \frac{\rho_{\text{on}}}{\rho_{\text{off}}} \quad (4)$$

The logarithm can be approximated by its expansion in power series up to first order:

$$\ln \frac{\rho_{\text{on}}}{\rho_{\text{off}}} \approx \frac{\rho_{\text{on}} - \rho_{\text{off}}}{(\rho_{\text{on}} + \rho_{\text{off}})/2} \equiv \frac{\delta \rho}{\rho} \quad (5)$$

which corresponds to the relative difference of the reflectances, here named as  $\delta \rho / \rho$ .

## 2.2 Laser footprint upscaling

The DLR airborne system TROPOLEX, used in this study, provides a high spatial resolution of the ground reflectivity composed of single footprints having a diameter below 10 m along the ground track of the aircraft with a footprint distance of about 10 m. In order to transfer the obtained lidar reflectance data to systems with larger footprints, the measurement data have to be upscaled. Conceivable satellite systems using the IPDA technique will provide laser ground spot diameters in the order of several tens of meters. Several approaches for an appropriate upscaling procedure are shown in the following. A comparison and a discussion are given in Sect. 6.

### 2.2.1 1-D upscaling

The first method is what we call 1-D upscaling. To account for the larger beam size of a spaceborne IPDA instrument, the measured lidar reflectivity data are averaged. In principle the required averaging is 2 dimensional, but measurements are available only in one direction, the aircraft track. The 1-D upscaling approach is calculated like a running average along the aircraft track. So the original resolution of the data is maintained. The upscaled reflectivity  $\rho^{\text{upsc}}$  is calculated by:

$$\rho_i^{\text{upsc}} = \frac{1}{n} \sum_{j=i}^{i+n-1} \rho_j \quad (6)$$

with  $\rho$  as the measured lidar reflectivity, the number  $n$  of averaged measurement shots. The calculations shown here base on an assumed footprint diameter of a spaceborne instrument of about 100 m, i.e.  $n = 11$ .

An alternative is to multiply an optional weighting function  $g$  to the reflectivity values within each ‘‘ground spot’’ interval to consider a beam intensity profile deviating from a top hat profile:

$$\rho_i^{\text{upsc},w} = \frac{\sum_{j=i}^{i+n-1} g_j \rho_j}{\sum_{j=i}^{i+n-1} g_j} \quad (7)$$

Here, a gaussian weighting with a FWHM of 38 m was assumed.

The relative reflectivity difference  $(\delta \rho / \rho)^{\text{upsc}}$  that is needed to yield the retrieval error can be calculated accordingly to Eq. (5) using consecutive values  $\rho_i^{\text{upsc}}$  and  $\rho_{i+1}^{\text{upsc}}$  which shall represent online and offline measurements of an IPDA system, that operates in the double pulse mode, emitting online and offline pulse pairs with small temporal separation (as suggested for A-SCOPE, see Sect. 8).

### 2.2.2 Auto-correlation method

The Auto-correlation method is a more rigorous two-dimensional upscaling method, but only allows access to limited information. It uses the auto-correlation of the reflectivities measured by TROPOLEX, which is calculated for a set of  $N$  data points with

$$C_{1-D}(x_i = i \cdot \delta x) = \frac{\sum_{j=1}^{N-100} \delta \rho_j \delta \rho_{j+i}}{\sum_{j=1}^{N-100} \delta \rho_j \delta \rho_j} \quad (8)$$

$$\delta \rho_j = \rho_j - \frac{1}{N} \sum_{k=1}^N \rho_k$$

$$0 \leq i \leq 100$$

$\delta x$  is the spatial sampling distance between two successive measurements, and the value of 100 has been chosen as being large enough to provide information about  $C_{1-D}$  over the spatial scale of interest, while being an order of magnitude smaller than  $N$ . Provided a sufficiently large dataset is used,  $C_{1-D}$  is a smooth function, thanks to the averaging along the aircraft track involved in its calculation. The calculated auto-correlation function can be extended to two dimensions, using only the assumption of isotropy:

$$C_{2-D}(r_i = i \cdot \delta x, \varphi) = C_{1-D}(x_i = i \cdot \delta x) \quad (9)$$

The equivalent 2-D autocorrelation function  $C_{2-D\text{avg}}(r_i, \varphi)$  that corresponds to the upscaled reflectivities can be calculated from  $C_{2-D}(r_i, \varphi)$  and, as will be shown, useful information about the statistics of the upscaled reflectivities can be extracted from it. To present the principles behind its calculation, expressions involving continuous functions are used. The use of discrete valued functions would involve more complicated notations, but is equivalent. It is assumed that the reflectivity upscaled to a larger laser footprint  $\rho_{2-D\text{avg}}(x, y)$  can be expressed as the following integral involving the TROPOLEX reflectivity  $\rho(x, y)$  and an averaging function  $B(x, y)$  that describes the spatial distribution of laser light within the beam:

$$\rho_{2-D\text{avg}}(x, y) = \iint \rho(x_0, y_0) B(x_0 - x, y_0 - y) dx_0 dy_0 \quad (10)$$

$B(x, y)$  is normalized as follows

$$\iint B(x_0, y_0) dx_0 dy_0 = 1 \quad (11)$$

In principle Eq. (11) should also include a deconvolution to correct from the finite size of the TROPOLEX beam. Due to the significantly larger A-SCOPE beam footprint, this additional step has a negligible impact and is not considered in the paper.

$\delta\rho(x, y)$  and  $\delta\rho_{2-\text{Davg}}(x, y)$  denote the differences between the reflectivities  $\rho(x, y)$  and  $\rho_{2-\text{Davg}}(x, y)$  and their mean values calculated by a spatial average into the full 2-D plane. Then

$$\delta\rho_{2-\text{Davg}}(x, y) = \iint \delta\rho(x_0, y_0) B(x_0 - x, y_0 - y) dx_0 dy_0 \quad (12)$$

This last result can be written

$$\delta\rho_{2-\text{Davg}}(x, y) = \delta\rho(x, y) * B(-x, -y) \quad (13)$$

$$\delta\rho_{2-\text{Davg}}(-x, -y) = \delta\rho(-x, -y) * B(x, y)$$

The autocorrelation function of the averaged reflectivity is

$$C_{2-\text{Davg}}(x, y) = K \iint \delta\rho_{2-\text{Davg}}(x_0, y_0) \quad (14)$$

$$\delta\rho_{2-\text{Davg}}(x + x_0, y + y_0) dx_0 dy_0$$

$$C_{2-\text{Davg}}(x, y) = K [\delta\rho_{2-\text{Davg}}(-x, -y) * \delta\rho_{2-\text{Davg}}(x, y)]$$

$$C_{2-\text{Davg}}(x, y) = K [\delta\rho(-x, -y) * \delta\rho(x, y)]$$

$$* [B(-x, -y) * B(x, y)]$$

$$C_{2-\text{Davg}}(x, y) = K C_{2-\text{D}}(x, y) * [B(-x, -y) * B(x, y)] \quad (15)$$

where the normalization factor  $K = 1 / \iint [\delta\rho_{2-\text{Davg}}(x_0, y_0)]^2 dx_0 dy_0$  allows to ensure, that  $C_{2-\text{Davg}}(0, 0) = 1$ .

All the information to calculate  $C_{2-\text{Davg}}$  is available. The averaging function  $B$  is usually analytical (a circular hat and a Gaussian will be considered in our work) so that  $B * B$  can be calculated analytically. Thus, only one 2-D numerical convolution is required. The variance  $\text{Var}(\Delta\rho_{2-\text{Davg}}, i)$  of the reflectivity change between two points separated by the distance  $i \cdot \delta x$  can be obtained from  $C_{2-\text{Davg}}$  as follows

$$\text{Var}(\Delta\rho_{2-\text{Davg}}, i) = \frac{1}{M} \sum_{j=1}^M (\rho_{2-\text{Davg}, j+i} - \rho_{2-\text{Davg}, j})^2 \quad (16)$$

$$\text{Var}(\Delta\rho_{2-\text{Davg}}, i) = \frac{1}{M} \sum_{j=1}^M [\delta\rho_{2-\text{Davg}, j+i}^2 + \delta\rho_{2-\text{Davg}, j}^2$$

$$- 2\delta\rho_{2-\text{Davg}, j} \delta\rho_{2-\text{Davg}, j+i}]$$

$$\text{Var}(\Delta\rho_{2-\text{Davg}}, i) = 2\text{Var}(\rho_{2-\text{Davg}})[1 - C_{2-\text{Davg}}(i \cdot \delta x)]$$

### 2.2.3 Upscaling method for sea surfaces

The sea surfaces measured by TROPOLEX were found to have a very short correlation length, clearly smaller than the measurement sampling distance (see Sect. 7.2). In this context, a model will now be built to describe the upscaling of un-correlated reflectivities. It aims to improve the reliability of the upscaling procedure and to get a better understanding of the measurements. First, it is assumed that the correlation length of the lidar reflectivity is much smaller than any distance considered in our treatment. For convenience, we will formally define a lidar reflectivity  $\rho(x, y)$  at every location  $(x, y)$ , being fully uncorrelated in the spatial dimensions. This reflectivity function, once averaged within the footprint where the spatial distribution of laser light is  $B(x, y)$ , becomes

$$\rho_{B,i} = \iint \rho(x, y) B(x - x_i, y) dx dy \quad (17)$$

where  $B(x, y)$  is assumed to be still normalized according to Eq. (11).

As  $\rho(x, y)$  is spatially uncorrelated, its variance over the area  $dS + dS'$  is equal to its variance over  $dS$  plus its variance over  $dS'$ . Extending this property to a finite area  $S$  gives

$$\text{Var} \left[ \iint \rho(x, y) dx dy \right] = \iint \text{Var}[\rho(x, y)] dx dy \quad (18)$$

It is now also assumed that  $\text{Var}[\rho(x, y)]$  does not depend on  $x$  and  $y$ . Then

$$\text{Var} \left[ \iint \rho(x, y) dx dy \right] = kS \quad (19)$$

where  $k$  denotes the constant variance and  $S$  is the surface of the finite area. This reasoning can be repeated with the product  $\rho(x, y)B(x - x_i, y)$ , by considering that  $dS$  and  $dS'$  are infinitesimal areas where  $B(x - x_i, y)$  is constant. Then

$$\begin{aligned} \text{Var}(\rho_{B,i}) &= \text{Var} \left[ \iint \rho(x, y) B(x - x_i, y) dx dy \right] \quad (20) \\ &= \iint \text{Var}[\rho(x, y) B(x - x_i, y)] dx dy \end{aligned}$$

Using Eq. (19), the following result is obtained

$$\text{Var}(\rho_{B,i}) = k \iint B^2(x - x_i, y) dx dy \quad (21)$$

In practice the reflectivity will not be uncorrelated, and will have a finite, even if quite small, correlation length. It is assumed in the paper that the areas  $dS$  and  $dS'$  where  $B(x, y)$  is constant are significantly larger than the correlation length. Then the result of Eq. (21) is still applicable for real cases.

$\text{Var}(\rho_{B,i})$  is now evaluated in two cases. For a top hat circular footprint, it is simply inversely proportional to the area  $S$ . The upscaling of the variance from the TROPOLEX beam with area  $S_0$  to a larger beam with area  $S_1$  is

$$\text{Var}(\rho_{S_1,i}) = \text{Var}(\rho_{S_0,i}) \frac{S_0}{S_1} \quad (22)$$

For a Gaussian beam the variance is

$$B(x, y) = \frac{1}{2\pi\sigma^2} \exp\left(-\frac{x^2 + y^2}{2\sigma^2}\right) \quad (23)$$

$$\text{Var}(\rho_{B,i}) = \frac{k}{4\pi\sigma^2}$$

The upscaling from a TROPOLEX Gaussian beam with  $\sigma_0$  to a space borne lidar with  $\sigma_1$  is given by

$$\text{Var}(\rho_{B_1,i}) = \text{Var}(\rho_{B_0,i}) \frac{\sigma_0^2}{\sigma_1^2} \quad (24)$$

Now the variance of the difference between  $\rho_{B,i}$  evaluated at two different points (denoted by  $i$  and  $j$ ) is calculated, as the function of the separation distance  $L$  between the two footprints. Depending on the value of  $L$ , there can be some overlap between the two footprints and the result needs to account for this possibility.

$$\begin{aligned} \text{Var}[\Delta\rho(L)] &= \text{Var}[\rho_{B,j} - \rho_{B,i}] \quad (25) \\ &= \text{Var}\left(\iint \rho(x, y)[B(x-L-x_i, y) - B(x-x_i, y)] dx dy\right) \\ &= k \iint [B(x-L, y) - B(x, y)]^2 dx dy \end{aligned}$$

For a top hat circular footprint with radius  $R_1$  and area  $S_1$  the expressions simplify. They explicitly include the fraction  $O(L)$  of the area  $S_1$  that overlaps with the second footprint, defined such that  $O(0) = 1$  and  $O(2R_1) = 0$ .

$$O(L) = \begin{cases} \frac{2}{\pi} \arccos\left(\frac{L}{2R_1}\right) - \frac{L}{\pi R_1} \sqrt{R_1^2 - \frac{L^2}{4}} & \text{if } L \leq 2R_1 \\ 0 & \text{if } L \geq 2R_1 \end{cases} \quad (26)$$

$$\text{Var}[\Delta\rho(L)] = 2\text{Var}(\rho_{S_1,i})[1 - O(L)] \quad (27)$$

For a Gaussian footprint defined with parameter  $\sigma_1$  we find

$$\text{Var}[\Delta\rho(L)] = 2\text{Var}(\rho_{B_1,i}) \left[1 - \exp\left(-\frac{L^2}{4\sigma_1^2}\right)\right] \quad (28)$$

These two expressions, applicable for the uncorrelated reflectivities observed over sea, have a similar structure as the results obtained in Sect. 2.2.2 with the auto-correlation method.

### 3 Experimental setup

#### 3.1 Instrument

The lidar system employed in this study is the DLR's TROPOLEX system (Meister et al., 2003), which is designed for use on board the DLR research aircraft Cessna Grand Caravan 208B (D-FDLR) as shown in Fig. 1. It consists of a laser system, a down-looking receiving unit and a data acquisition unit. Some modifications of the original system which was designed for the measurement of tropospheric

ozone were necessary for this study. The modified system provides 5 mJ per pulse at 1.573  $\mu\text{m}$  wavelength with a 10 Hz repetition rate. The output power is monitored for the relative calibration of the outgoing pulses. Table 1 summarizes the main parameters of the system.

Figure 2 shows the layout of the system. It operates in bistatic configuration, with a laser transmitter and a separate receiving telescope. A flashlamp pumped Nd:YAG laser operating at its fundamental frequency (1.064  $\mu\text{m}$ ) is used to pump an optical parametric oscillator (OPO) (Giordmaine and Miller, 1965; Tang et al., 1992) with a KTP-crystal as the non-linear medium (size:  $5 \times 5 \times 20 \text{ mm}^3$ ). The OPO converts the 1.064  $\mu\text{m}$ -radiation into 1.573  $\mu\text{m}$  (signal) and 3.3  $\mu\text{m}$  (idler). The idler radiation is not used here. A small part of the signal radiation is picked up and guided to an integrating (Ulbricht) sphere, where an InGaAs-PIN-diode is installed for the power reference measurement of each laser pulse. The outgoing beam diameter is about 1 cm and adjusted to a beam divergence of 3 mrad. The beam is guided downwards out of the aircraft. There is a constant off-nadir angle of about 1.2° to the forward direction in addition to temporally occurring roll and pitch angle variations of the aircraft. A down-looking Cassegrain type telescope (4 mrad field of view) collects the light backscattered by the ground. Then it is focused on a diffusor and imaged onto the detector. This diffusor considerably enhances the signal stability. A second InGaAs PIN diode (1 mm diameter of the active area) serves as the detector. A polarization filter can be inserted into the receiver light path and removed during the measurements (transmission 98%, contrast >10 000:1). It is adjusted orthogonally to the outgoing laser beam polarization. So the depolarized part of the backscattered light can be detected. Here, the filter was only used in some selected cases (see Sect. 7.3). The major part of the measurements was performed without the filter.

Additionally, there are two cameras installed for monitoring the ground area around the telescope's field of view: one operating in the visible spectrum and another one in the near IR, limited by a bandpass filter to the range between 1500 nm and 1600 nm. The captured pictures are used to identify the ground surface types.

The employed Cessna Grand Caravan 208B is an one engine turboprop aircraft that provides special apertures at the bottom side of its body for the use of down-looking scientific instruments. It provides a non-stop range of more than 1000 km and can be used for overflights of the sea up to 10 km offshore. The flight altitude above ground during the measurements was between 1.5 and 3 km, the ground speed was between 290 km/h and 360 km/h.

#### 3.2 Measured data

The collected raw data contain the output-power monitor data, the ground reflex data and the distance to the ground calculated from the laser pulse runtime. Due to the short



**Fig. 1.** TROPOLEX system installed on the DLR research aircraft Cessna Grand Caravan.

pulse response width of the detector/preamplifier system (80 ns FWHM) spatially structured targets, such as trees, cause temporally structured return signals. To compensate for this effect, lidar reflectivity data are calculated by integrating the whole pulse return that is detected in the detector sampled signal.

The ground reflex data are normalized by the corresponding output-power data. Additionally, the ground reflex data are corrected with respect to ground distance variations that occur due to the orography and aircraft altitude changes. The resulting quantity (named as  $\rho$ , in arbitrary units) is assumed to be proportional to the absolute lidar ground reflectance  $\rho^*$  (in  $\text{sr}^{-1}$ ). Additionally the data are geo-referenced using an on-board differential GPS system. Furthermore, data about the aircraft attitude are available.

In order to avoid interferences introduced by the absorption of  $\text{CO}_2$  and  $\text{H}_2\text{O}$  to keep the focus on the ground reflectivity only, the OPO was operated in a broadband mode with a spectral bandwidth of the generated radiation of 0.2 nm. This is much broader than the absorption lines of water vapor and carbon dioxide that occur in this wavelength region and so there is no significant absorption. Numerical simulations showed, that absorption changes due to variations of the  $\text{CO}_2$  and  $\text{H}_2\text{O}$  concentrations or of the flight altitude as

**Table 1.** Technical Parameters of the system.

Transmitter	
wavelength	1573 nm
bandwidth	0.2 nm FWHM
energy per pulse	5 mJ
pulse length	5 ns
repetition rate	10 Hz
source	Nd:YAG pumped KTP-OPO system
beam divergence (full width)	3 mrad
Receiver	
telescope type	Cassegrain, 35 cm diameter
detector	InGaAs PIN (1 mm active area diam.)
field of view (full width)	4 mrad
data acquisition	12-bit, 400 MHz digitizer
pulse response width	80 ns FWHM
vertical resolution	12 m
Geometry	
down-looking, with off-nadir angle	1.2° (to forward direction)
laser spot diameter on ground	5–9 m (depending on flight altitude)
distance between two spots	8–10 m (depending on speed)
Platform	
aircraft	Cessna Grand Caravan 208B
ground speed	290–360 km/h
aircraft to ground distance	1.5–3 km
possible non-stop flight range	> 1000 km

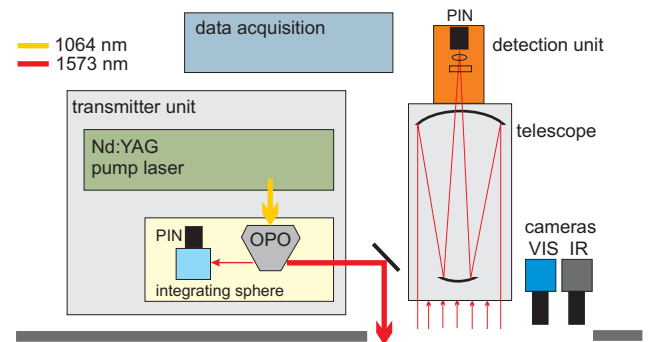


**Fig. 2.** TROPOLEX system layout for ground reflex measurements.

well as possible wavelength instabilities lead to deviations in the order of the instrumental noise and so, do not have a noticeable influence on the ground reflectivity measurement.

The beam attenuation due to atmospheric aerosol scattering and absorption was not corrected, since the main focus of this investigation was on the relative reflectivity variability in the order of several tens of meters, on which no significant changes of the aerosol load is expected.

The typical laser footprint diameter on ground is 5 m to 9 m depending on the distance from the aircraft to the ground. The center-to-center distance between two consecutive footprints is between 8 m and 10 m, depending on the aircraft ground speed. So normally there is no overlap and an almost continuous capture of the ground reflectivity with a high spatial resolution is achieved.

**Table 2.** Instrumental noise analysis results with respect to all quantities derived from the measurement data.

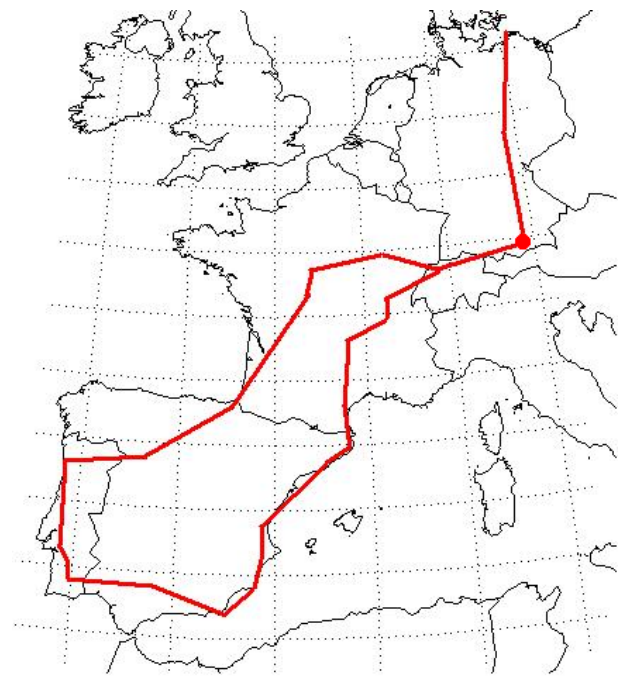
Quantity	Basis	Precision (RMS)
target distance	–	1 m
TROPOLEX reflectivity $\rho$	original	1.9%
	1-D upscaled (100 m)	0.6%
absolute reflectance $\rho^*$	original	0.003 $\text{sr}^{-1}$
	1-D upscaled (100 m)	0.001 $\text{sr}^{-1}$
reflectivity difference $(\delta\rho/\rho)_{10\text{m}}$	original	2.7 percentage points
	1-D upscaled (100 m)	0.24 percentage points
A-SCOPE $\text{CO}_2$ error	1-D upscaled (100 m) and averaged over 350 measurements	0.02 ppm (0.005%)

An analysis of the TROPOLEX's instrumental noise was performed by means of a reference measurement in the laboratory using a stationary and defined target with a flat and homogeneous surface: a wall made of construction concrete in 100 m distance to the system. Due to the comparable short distance to the target possible atmospheric influences are not considered here. So, only the instrumental noise appears. Table 2 shows the results for all quantities that are derived from the measurement data (the definitions are given in the respective sections). The values given here are calculated using the same routines as used for the analysis of the airborne measurements. The values of the absolute reflectance precision base on a calibration using ASTER spectral library data (Baldrige et al., 2009). Since the detector/preamplifier noise is well below the obtained values, it is assumed that the noise is mainly caused by electromagnetic interference due to the high voltages of the laser's q-switch and by an imperfect power reference measurement which turned out to be critical in previous measurements (Amediek et al., 2008).

#### 4 Measurements

The measurement flights performed during this project provide data covering more than 5000 km ground track length (see Fig. 3). From these data, 25 flight legs have been extracted with individual lengths between 30 and 340 km, and an overall length of more than 3300 km, each providing continuous data without interruptions due to cloud coverage or other reasons. Several local flights during different seasons took place in the alpine upland close to Oberpfaffenhofen airfield (Southern Germany). Long range flights to the Baltic Sea across Germany and to Spain via France and Portugal yield data from different regions with various terrains. Flights over the Baltic Sea as well as the Mediterranean Sea offer data about the sea surface reflectivity.

The flights took place in December 2007, April and June 2008. They cover grasslands, forests, different agricultural landscapes, lakes, the open sea, partly snow covered terrains, mountainous and rocky areas, very dry regions with sparse vegetation and urban areas. Most types of arid and humid

**Fig. 3.** Tracks of the performed flights in Central and Western Europe.

regions occurring in Central and Western Europe were captured.

The Figs. 4 and 5 show typical measurement results collected during the flight missions. In the upper part of each plot the aircraft to ground distance is depicted, the middle part shows the non-averaged reflectivity (10 m horizontal resolution) and at the bottom a quality flag indicates, that single values are skipped at the respective positions (a vertical peak upwards in the case of detector overload or clouds, downwards in the case of a very weak signal). A second y-axis on the left side indicates absolute reflectances  $\rho^*$ , obtained by using MODIS data along the respective flight tracks (see also Sect. 5).

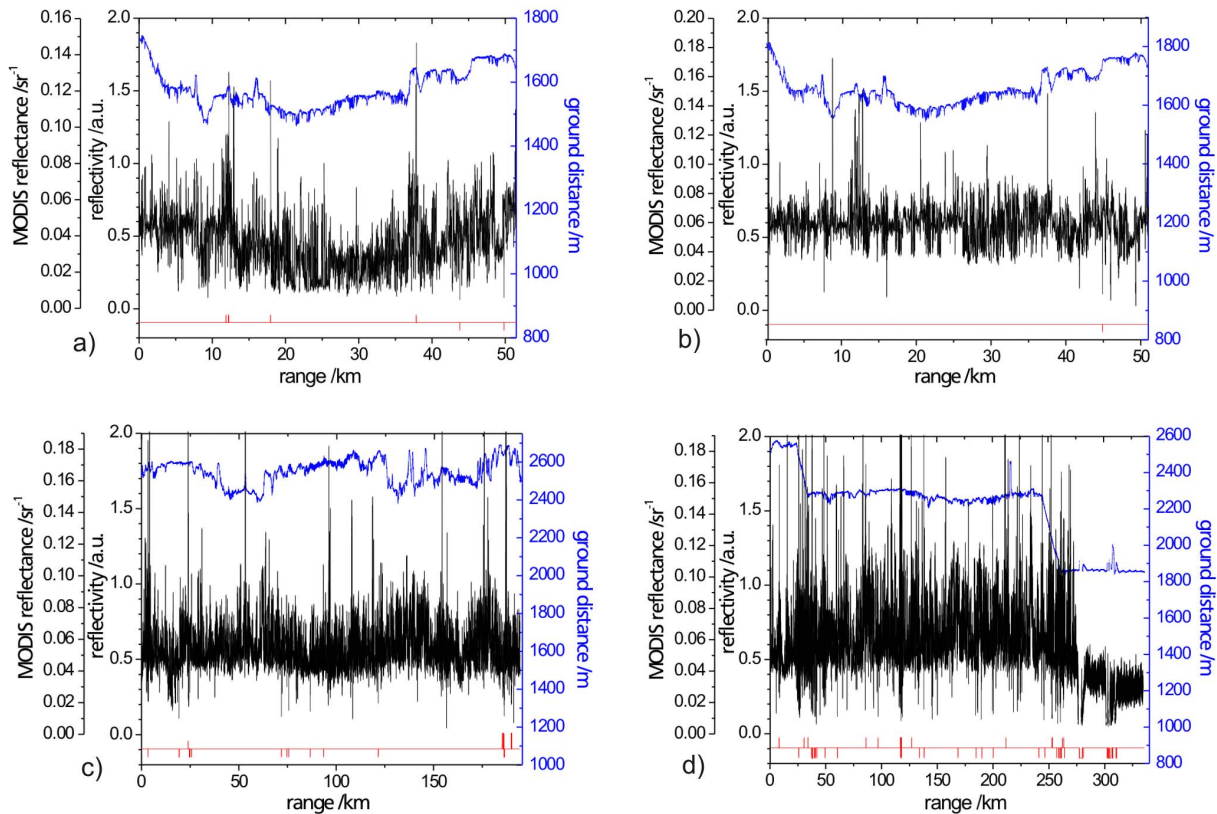


**Fig. 4.** Measurement data: (a) Southern Germany (April 2008, partly snow covered), (b) same route as in (a) (June 2008), (c) Southern Germany (April 2008), (d) Northern Germany (April 2008).

The plots a) and b) of Fig. 4 show two measurements of the same 50 km track, performed in April and June, as demonstrated by the ground distance curve showing an identical orography signature. These data show the same terrain during different seasons: before the vegetation period with patches of old snow in April, and at the beginning of the vegetation period in June. The reflectivity measured in April is significantly decreased in the middle part of the leg, where the snow patches occurred.

The flight across Germany to the Baltic sea (April) is plotted in c) (Southern Germany) and d) (Northern Germany) of Fig. 4. At kilometer 275 in plot d) the coast was crossed to the open sea. The landscape in Southern Germany is dominated by small structures (farmland, forest, populated areas), while Northern Germany shows more large scale structures (less forests, more and larger agricultural fields).

Figure 5 displays flight legs in Portugal and Spain (a–c) and Southern France (d) measured in June. In general the ground surface in Spain is dryer than in France and Germany. Plot a) in South-West Spain represents an area, that is dominated by agricultural fields and forests. Plot b) depicts a 630-km flight leg with different surface types in Southern Spain: large olive groves at the beginning, the mountains of the Sierra Nevada, then a very arid section, the Mediter-

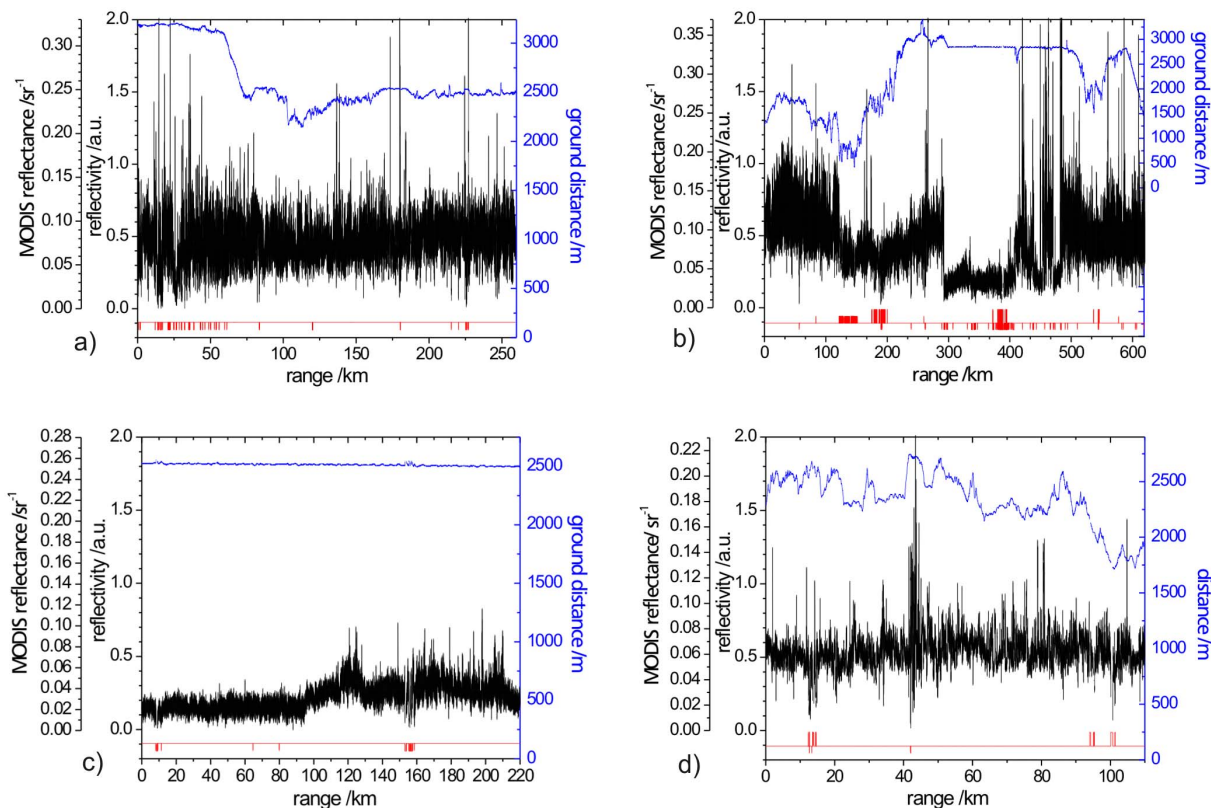
ranean Sea, a section with inland water bodies (Mar Menor close to Murcia, known for its smooth surface) alternating with land and several crossings of the costal line, and at the end again mountainous terrain and partly farmed ground (see also Fig. 7). Plot c) shows a flight leg over the Mediterranean Sea and plot d) a region in Southern France dominated by agricultural land and forests.

Figure 6 shows a 9-km-zoom into the flight performed in April 2008 (Southern Germany) to give an impression of the small scale reflectance variability. This example contains snow covered grassland sections, a small settlement and forests that have parts sparsely covered with trees. The lower panel depicts the relative reflectivity differences  $\delta\rho/\rho$ .

## 5 Absolute reflectances using MODIS and Cox & Munk

### 5.1 Comparison to MODIS data

The TROPOLEX system itself is not able to provide absolute lidar reflectance data, but a calibration by means of external data can be performed, for example using satellite data from passive sensors. The connection between the data sets can be done by using the geo-location information. Here, the collected imaging data are compared to band 6 data of the



**Fig. 5.** Measurement data, June 2008: (a) Portugal, (b) Southern Spain (including Mediterranean Sea), (c) Mediterranean Sea, (d) Southern France.

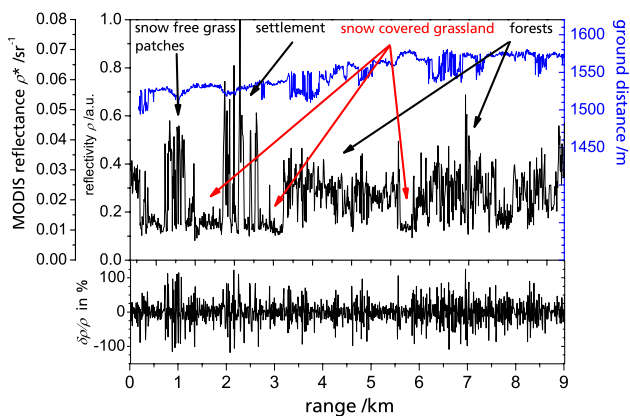


**Fig. 6.** 9-km-zoom taken from an April flight (Southern Germany); 10 m horizontal resolution, no footprint upscaling; upper panel: ground distance (blue) and TROPOLEX ground reflectivity (black); corresponding reflectances  $\rho^*$  taken from MODIS data as a second y-axis; lower panel: relative reflectivity differences  $\delta\rho/\rho$ ; forest areas can be identified by the signatures in the ground distance.

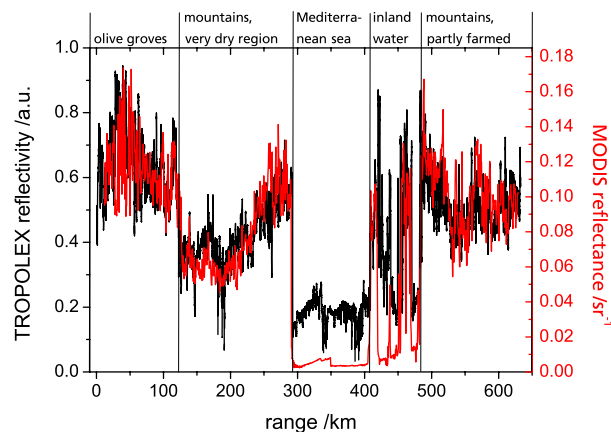


**Fig. 7.** Flight leg in Southern Spain (June 2008): TROPOLEX measurement data (500 m averages) and corresponding MODIS data for the same ground track (500 m pixel size).

Moderate Resolution Imaging Spectroradiometer (MODIS) on board the Terra and Aqua satellites which provides land surface reflectance data in the spectral range between 1628 nm and 1652 nm, thus close to the TROPOLEX wavelength. Here, mainly the data product MOD09A1 (level-3, 8-day composites, 500 m spatial resolution, aerosol corrected) was used (Justice et al., 2002).

The following section describes the connection of TROPOLEX data with MODIS data to get an access to absolute reflectance values at the TROPOLEX's spatial resolution of 10 m, thus far below the resolution of MODIS. Furthermore the lidar reflectance of the sea surface can be determined, which is not provided by MODIS.

Figure 7 shows again the 630-km flight leg between Cordoba and Valencia in Southern Spain. Here, both TROPOLEX and MODIS data are plotted for the same ground track. The TROPOLEX data are averaged along 500 m to get a spatial resolution closer to the MODIS data. The scale of the MODIS reflectance data is linearly stretched, so that the best possible matching is achieved for the whole flight (by eye). This method allows to determine a kind of calibration factor. Those factors are valid only for single measurement flights, since after each landing and re-takeoff an adjustment of the beam/telescope overlap was performed. These re-adjustments do not lead to exactly reproducible results.

In general, there is a good relative agreement of the different datasets, but it has to be mentioned, that the comparability of the different data, and so a calibration, is not automatically given. One point is, that a  $(500 \times 500) \text{ m}^2$  MODIS pixel is compared to the narrow TROPOLEX ground track. So dependent on the heterogeneity of the respective surface structure the TROPOLEX data are expected to show a higher variability. Another aspect is the difference in the wavelength regions, which cause higher MODIS values, between 1.5% and 15%, compared to TROPOLEX measurements depending on the surface type (according to ASTER). Furthermore the lidar configuration always measures the "hotspot" (view angle is equal to the light incident angle) (Hapke et al., 1996; Bréon et al., 2002), whereas the MODIS measurement geometry normally differs from this particular case, since the MODIS viewing angle related to the sun zenith angle is variable. For most surface types this leads to higher TROPOLEX values (see below). Changes of the aerosol load of the atmosphere within a flight leg could also lead to deviations. By means of numerical simulations on the basis of the ESA Reference Model of the Atmosphere (Ehret et al., 2005) the decrease in the measured ground reflectivity along with an increase in the aerosol load was estimated for the given measurement configuration. Assuming an increase of the vertical aerosol content corresponding to a change from the "lower quartile aerosol model" to the "median aerosol model" (the titles refer to the statistical occurrence of the respective atmospheric conditions) a decrease in the measured ground reflectivity of 15% results. The quality of the MODIS data is

validated by Liang et al. (2002). In their test measurements they found an error of less than 5%. Due to the unknown contributions of the mentioned points no corrections were made at this stage of the data analysis and so the calibration has still an unknown uncertainty.

## 5.2 Land and sea surfaces reflectances

In the next step, those land surface types were identified that show the minimum and maximum reflectances. Snow covered grassland areas (observed in Southern Germany) are identified to show the lowest reflectance of all solid surfaces:  $\rho^* = 0.012 \text{ sr}^{-1}$  (average value). The highest reflectance was found in Southern Spain and identified as dry grass (in olive groves):  $\rho^* = 0.18 \text{ sr}^{-1}$  (average value). These values obtained using the direct MODIS calibration, as shown above, are in good accordance to the data of the ASTER spectral library. Single measurement points can exceed these limits considerably as shown in the discussion about the dynamic range below. Furthermore, reflectance changes also on small spatial scales, are mostly reproduced with good relative accordance between TROPOLEX and MODIS, as can be seen in Fig. 8. It also indicates, that the Nadir BRDF-adjusted reflectance MODIS product MCD43A4 shows no significant differences compared to MOD09A1.

One important result of this study is the fact, that on average the observed sea surface reflectivity level is almost one half of the level that is obtained over land. Noticeable differences in the sea reflectance level during a flight often could be correlated with observable differences of the sea surface structure (recorded by the vis-spectrum-camera).

All flight legs that contain sea overflights can be calibrated using the land surface information within the same flight to get the absolute reflectance by means of MODIS data. In this way a reflectance of the sea surface between  $0.02 \text{ sr}^{-1}$  and  $0.05 \text{ sr}^{-1}$  was derived (on the basis of 1-km averages to smooth the small scale variations). The wind speeds during the corresponding measurements were quite low, between 2 m/s and 5 m/s without whitecaps.

## 5.3 Comparison to Cox & Munk and discussion

A noticeable discrepancy occurs, if the mentioned sea surface reflectances, obtained by the direct calibration of the TROPOLEX data to MODIS data, are compared to the expected reflectances calculated on the basis of Cox and Munk (1954). Here, values between  $0.045 \text{ sr}^{-1}$  and  $0.125 \text{ sr}^{-1}$  result for the conditions that were existent during the measurements (wind speed and off-nadir angles between  $1^\circ$  and  $5^\circ$  due to the aircraft attitude). That would indicate an underestimation of the MODIS calibrated measurements, if it is performed as described above, by a factor of up to 2. The most probable reason for this disagreement is the hotspot effect. Camacho-de Coca et al. (2004) investigated this effect for different agricultural crops in the spectral range between

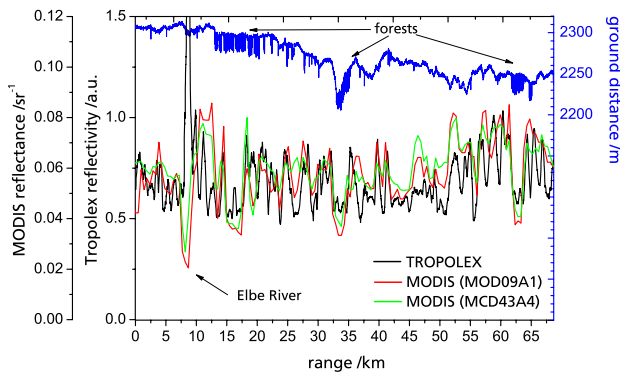


**Fig. 8.** Zoom into data from Northern Germany (April 2008): TROPOLEX (500 m averages) and MODIS data (500 m pixel size, ground reflectance MOD09A1 and Nadir BRDF-adjusted reflectance MCD43A4); landscape: forests alternating with agricultural fields just before the vegetation period (forests can be identified by the signatures in the ground distance).

440 and 2200 nm by airborne measurements. They observed at 1593 nm a hotspot reflectance enhancement factor around 1.6 for Alfalfa and Barley. Kaasalainen et al. (2006) investigated the hotspot peak properties for snow, Kaasalainen and Rauaiainen (2005) focus on lichens. Disney et al. (2009) provide a detailed investigation of the effect for different surface types especially for spaceborne IDPA measurements at 1.57  $\mu\text{m}$  and 2.05  $\mu\text{m}$ . They state enhancement factors between 1.1 and 1.3 depending on the surface type in mean. So, this effect could be an explanation of the discrepancy for the most part, which would mean, that the MODIS shown here data under-estimate the absolute lidar reflectance of the ground.

## 6 Comparison of the different upscaling approaches

A special flight was performed during this project to compare the various upscaling methods with real data in a case study. The flight pattern was arranged in a way, that the same 50-km route was flown 8 times very precisely using the aircraft Navigation System. Hereby, the single tracks have a distance of about 10 m to 20 m to each other, spaced orthogonally to the flight direction. So, by means of the geo-location information of the data a 2-D reflectivity array, with about 100 m in width, was obtained that allows the composition of larger footprints. The flight took place in April 2008 in the alpine upland in Southern Germany. The region is dominated by alternately occurring small forests, grassland and settlements. Due to the landscape characteristic and the fact that there were patches of old snow the reflectance variability was relatively high.

The upscaling to 100-m 2-D footprints is done as follows. Each single footprint is composed by cutting out a square from the data array (about 80 single measurements).

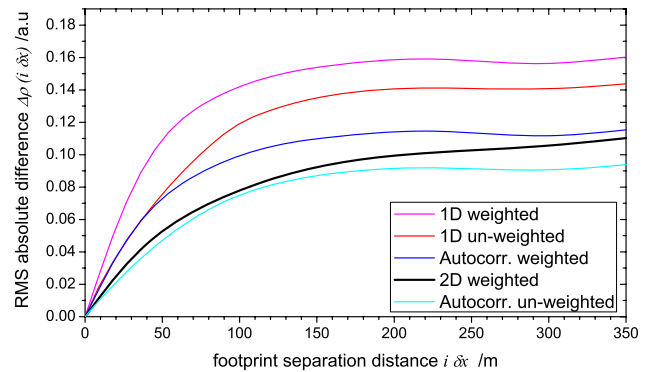


**Fig. 9.** Different upscaling approaches (100 m footprint diameter, un-weighted and gaussian weighted with 38 m FWHM) on the basis of 1-D measurement data compared to 2-D data (solid line, obtained by a special flight pattern).

Then, the data within such a square are weighted with a two-dimensional gaussian function with 38 m FWHM. This method allows to simulate the real footprint of a space borne laser system. The next footprint is calculated accordingly by using the array shifted by one row (10 m).

Figure 9 shows a comparison of the different upscaling approaches on the basis of this 50-km test route. The 1-D approaches use the information from the mid-track of the 2-D array. The plots depict the reflectivity differences depending on a variable spatial gap between two ground spots along the track. The resulting curves for the 1-D upscaled data (using un-weighted reflectivities  $\rho$ , according to Eq. (6), as well as Gaussian weighted, according to Eq. (7) and for the 2-D data (only Gaussian weighted) are calculated as follows

$$\Delta\rho_{j,i} = \rho_j - \rho_{j+i} \quad (29)$$

where the gap is represented by  $i \cdot \delta x$  (for  $\delta x \approx 10$  m). For each  $i$  corresponding to gaps between 0 and 350 m the resulting root mean square (RMS) values of  $\Delta\rho(i)$  are plotted on the basis of all measurements  $j$  along the 50-km-track section. The results of the autocorrelation method are calculated using Eq. (16).

In general one would expect, that the reflectivity differences calculated from 1-D upscaled data are overestimated noticeably compared to results from real 2-D footprints, since one can assume, that the averaging of the small scale differences using two dimensions causes a stronger smoothing. On the other hand consecutive reflectivity values show a correlation on short scales as shown in Sect. 7.2. So, the overestimation of the 1-D averaged reflectivities is not as strong as should be expected for uncorrelated data. The plots indicate that the 1-D upscaling overestimates the reflectivity differences compared to the 2-D data, as expected. The gaussian-weighted 1-D upscaling leads comparatively to high differences, whereas the un-weighted 1-D upscaling is more realistic. In general the weighting enhances the contribution of the footprint center. This is equivalent to a decrease

in the footprint size. As a result the averaging efficiency decreases.

The results from the autocorrelation approach are close to the 2-D results. The un-weighted case under-estimates the reflectance differences, as expected, and so it should not be used. The weighted case is expected to give the most accurate estimate of the real 2-D footprints. Its only assumptions are: isotropy and stationarity of the reflectance statistical properties. According to Fig. 9, there is however a slight discrepancy between the auto-correlation approach with weighted measurements and the real 2-D footprints. This could be explained by the observed fact, that the measured reflectivity increased slightly during the execution of the 2-D flight pattern, probably due to a drying of the surface in the morning.

In summary, the weighted autocorrelation approach is a precise estimation for upscaling 1-D track data to larger gaussian-weighted 2-D ground footprints, if the focus of the investigation is on the variance of absolute reflectivity differences. For the calculation of the IPDA retrieval error the use of relative differences is needed (see Sect. 2.1). For that purpose the un-weighted 1-D upscaling turns out to be an acceptable representative for gaussian-weighted 2-D footprints. It is easy to implement and each  $\delta\rho/\rho$  of consecutive ground spots along the flight track can be calculated. So, all results given in the following sections that refer to upscaled data base on the un-weighted 1-D upscaling. The overestimation of the reflectivity differences coming along with this approach involves, that the derived retrieval errors can be treated safely as upper bounds.

## 7 Characteristics of lidar ground reflectivity

### 7.1 Dynamic of the reflectivity

An important point for the design of a measurement system is the occurring signal dynamic which is in case of IPDA strongly dependent on the ground reflectances. The measurement sensitivity of the instrument should fulfill the requirements for all occurring ground reflectances as far as possible. Since Earth's ground albedo is highly variable in the visible spectrum, the lidar reflectance in the IR-range is suspected of being variable in the same manner, which is already indicated by the ground reflectance data of the ASTER spectral library (Baldrige et al., 2009) or MODIS (Justice et al., 2002).

The measurement data (see Figs. 4 and 5) confirm this assumption. Regarding all flights of this project, as the maximum contrast between the darkest and the brightest solid surface a factor of 15 was found for snow covered grassland in Southern Germany ( $0.012 \text{ sr}^{-1}$ ) compared with dry grass in Spain ( $0.18 \text{ sr}^{-1}$ ). If one looks onto the reflectivities of all single extracted flight legs (no upscaling), it results, that the corresponding RMS deviations from the respective means for different landscapes vary between 21% and 38%,

if no snow coverage occurred. Flight legs with partly snow covered ground in a region with a complex spatial structure on a small scale, like in Southern Germany (forests, grassland, agricultural fields, populated areas), showed the highest reflectivity dynamic with RMS deviations up to 90%. Figure 10 gives typical examples of the reflectivity distribution for different surface types. The plots shown in Fig. 11 base on the same data and depict the occurrence of the absolute reflectance differences  $\delta\rho^*$  dependent on the respective absolute reflectance. This figure indicates a possible dependency of the the rms reflectivity variations with respect to the reflectivity itself. In some case, the rms variations are found to be lower than the average in the limit of very low or very strong reflectivities. In principle, when calculating a radiometric budget for a lidar instrument, the value used for the reflectivity (that defines the measured signal and hence, shot noise) must correspond to the value used for the rms reflectivity variation (which defines overlap noise). In the paper, rms variations averaged over all values of the reflectivity are calculated and are assumed to be appropriate for most practical cases.

Another detail that is indicated by the measurements is the occurrence of single reflectivity extrema, which could exceed the surrounding reflectivity level considerably up to the detection limit of the system. By means of the down-looking cameras most of the surface types that come along with these cases could be identified. They occur cumulatively in urban areas, where a factor of up to 5 was typical for single extrema. Lakes and rivers can cause stronger outliers, resulting in both very weak as well as very high values, mostly alternating on a short spatial scale.

In addition to the reflectivity dynamic, the reflectivity changes on small scales must also be characterized since they can cause an IPDA retrieval error. This aspect is treated in the following.

### 7.2 Small scale reflectivity changes

Due to the high spatial resolution of the measurements a quantification of the reflectivity changes on short scales which could affect the IPDA measurement can be performed.

Figure 12 depicts the auto-correlation of the reflectivity (non-upscaled) for four exemplary flight legs with three different land use types and the open sea. The signal from the sea turns out to be totally uncorrelated, while the signals from the land surfaces show correlations with different grades. The figure confirms the expected connection between the apparent spatial structure of the land use type and the correlation length by trend. Nevertheless a classification is not possible, since the auto-correlation functions vary strongly, also for apparently similar surfaces. Figure 9 showed the behavior of the reflectivity differences depending on the spot separation distance. The non-linear increase is determined by the overlap of the ground spots (here upscaled) and by the correlation of the reflectivity along the track. The best

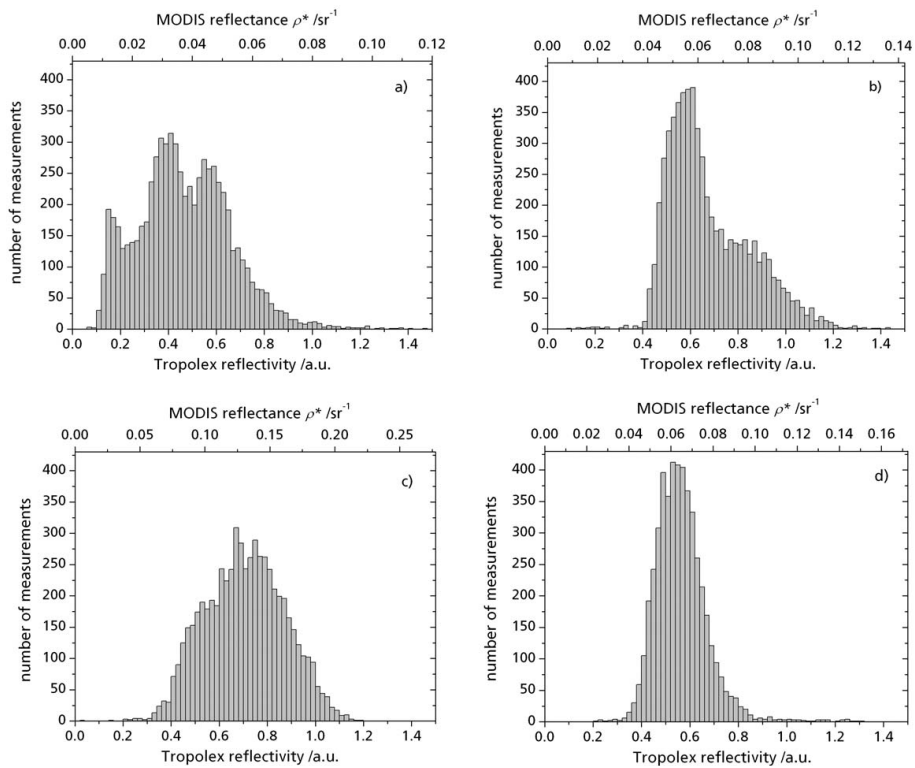


**Fig. 10.** Histograms of reflectivities  $\rho$  measured by TROPOLLEX taken from different regions in Europe (50-km sections each): **(a)** Southern Germany (April), **(b)** Northern Germany (April), **(c)** Spain, olive groves (June), **(d)** Southern France (June) (the shown MODIS data base on the calibration described in Sect. 5).

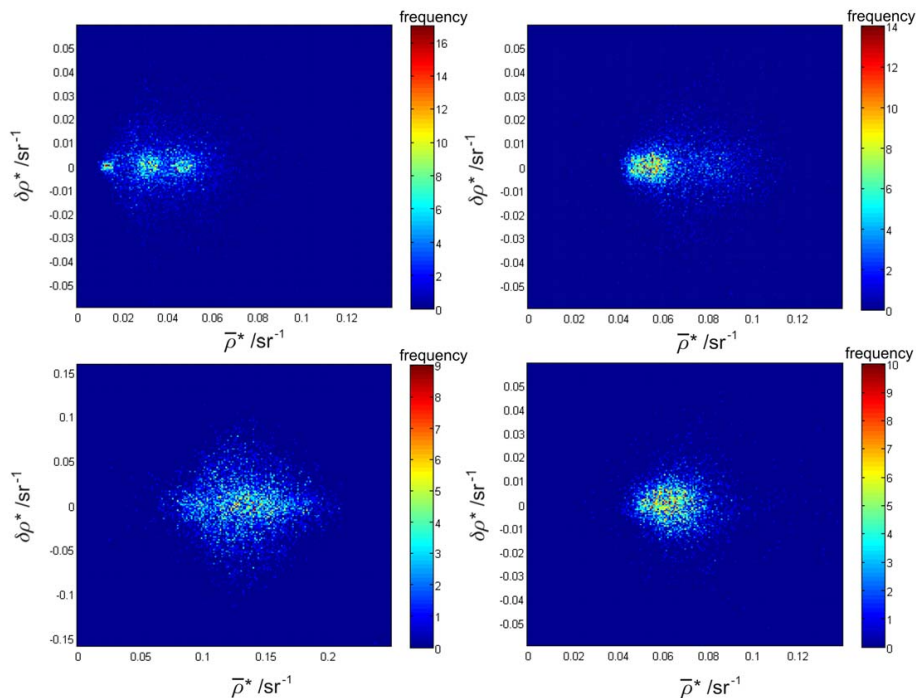


**Fig. 11.** Histograms of the absolute reflectance differences  $\delta\rho^* = \rho_i^* - \rho_{i+1}^*$  dependent on the respective absolute mean reflectance  $\bar{\rho}^* = (\rho_i^* + \rho_{i+1}^*)/2$  on the basis of the same data as used in Fig. 10 (absolute values base on the MODIS calibration according to Sect. 5).

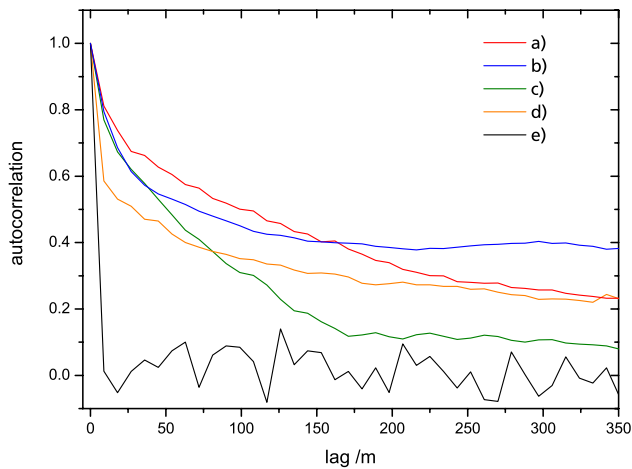


**Fig. 12.** Autocorrelations of the (non-upscaled) reflectivities  $\rho$  from different regions: **(a)** Northern Germany (agricultural fields – large structures); **(b)** Southern Germany (forests, fields – small structures); **(c)** Southern France (forests, fields – small structures); **(d)** Southern Spain (olive groves – fine structures); **(e)** open sea.

description of the curve shapes was obtained with exponential fits. Due to the non-linear characteristic a reflectivity gradient that allows a direct transfer to different spot separating distances is only possible for very short separating distances.

An example for the distribution of the reflectivity differences  $(\delta\rho/\rho)_{10\text{m}}$  (for 10 m spatial distance) is depicted in Fig. 13, calculated according to Eq. (5). Due to the isotropy of the ground surface structures the distribution is almost symmetrical with respect to zero. The mean reflectivity difference of the shown case (50 km flight leg, high variability due to partial snow coverage, about 6500 measurements) is 0.4%. Along with footprint upscaling the RMS of  $(\delta\rho/\rho)_{10\text{m}}$  reduces noticeably from 29.9% to 4.4%. Table 3 summarizes the minimum and maximum values for  $(\delta\rho/\rho)_{10\text{m}}$ , regarding all available flight data, each represented by RMS values on the basis of 50-km-sections.

The comparison of the same 50-km-ground track during different seasons showed a considerable increase of the  $(\delta\rho/\rho)_{10\text{m}}$  for the April-flight (with partial snow coverage) in comparison to the June-flight – in this particular case: 18% (June) and 29.9% (April) with respect to the original data; 2.5% (June) and 4.4% (April) with respect to the upscaled data. That shows, that a strong dependency of the retrieval precision on the season will result for some regions, especially if snow coverage occurs.

The RMS of the reflectivity deviations from flight legs over the sea varies between 12% and 27%. So, in general the variability (absolute as well as relative) was lower than over land surfaces. For sea surfaces the RMS of the reflectivity differences  $(\delta\rho/\rho)_{10\text{m}}$  for upscaled laser footprints (100 m) turned out to be small, between 0.36% and 0.82% (using Eq. 27). So, the homogeneity of the sea surface will

**Table 3.** Minimum and maximum reflectivity differences  $(\delta\rho/\rho)_{10\text{m}}$  found in the collected data set; RMS values for 50-km-sections; for non-upscaled original ground spots as well as 1-D up-scaled to 100-m footprints.

RMS <sup>50km</sup> $[(\delta\rho/\rho)_{10\text{m}}]$	upscaled	
	original	(100 m)
minimum	13%	2.2%
maximum (snow free)	24%	4.1%
maximum (partly snow covered ground)	54%	10%

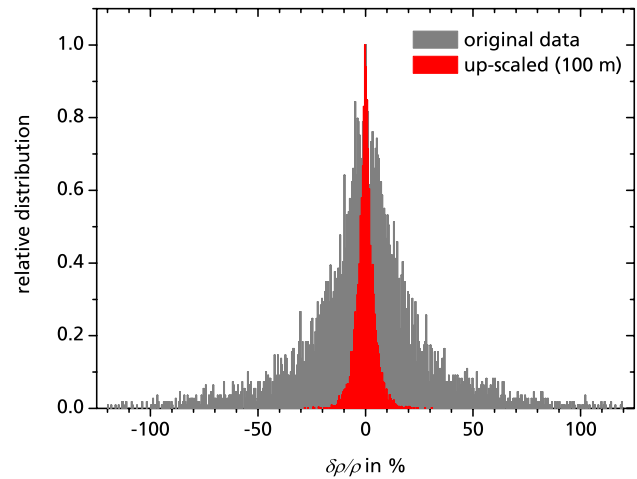


**Fig. 13.** Distribution of the relative reflectance differences  $\delta\rho/\rho$  (per 10 m) for a 50-km-flight leg (about 6500 measurements) in Southern Germany: the RMS of the non-upscaled data is 29.9%, of the upscaled data 4.4%; the distribution is almost symmetrical, the mean is 0.4% (bin size: 0.5%).

lead to smaller retrieval errors due to the online/offline footprint shift compared to land surfaces. However, the lower reflectance of the sea surface will lead to a lower signal to noise ratio.

### 7.3 Observation of polarization effects

This section reports about observations regarding the polarization of the laser ground reflex. Although there is no direct connection to A-SCOPE currently, the knowledge about this could be necessary for future designs of IPDA's receiving optics in terms of the usage of polarization sensitive optical parts.

Here, the application of the polarization filter in the receiving path allows the measurement of the depolarized part of the backscattered laser light. The first observation was, that for flight legs with inserted polarization filter the occurrence of the above mentioned high signal extrema was reduced considerably. So one can conclude that the high reflectivity cases often come along with a non-depolarizing backscatter,

e.g. due to a specular character of the corresponding surfaces. Nevertheless, the use of the polarization filter did not show any significant effects on the characteristics of  $\delta\rho/\rho$ , as indicated by the direct comparison of a special flight leg that was exactly flown twice, with and without the filter.

Furthermore no depolarization of the received light from the sea surface could be detected, as expected. Special flight manoeuvres, in which the aircraft's roll angle was varied, showed the expected dependency of the signal strength on the off-nadir angle (Bréon and Henriot, 2006). At a certain angle the signal completely dropped down to zero. Both facts confirm, that at this wavelength the received signal is dominated by specular surface reflection and there is no sub-surface backscattering within the range of the measurement sensitivity.

For land surfaces the signal amplitude, when using the polarization filter, was about one third compared to the signal without the filter (between 29% and 37%). A full depolarization of the polarized laser light by surface backscattering would lead to a signal amplitude of almost 50%. That indicates that the ground surface backscattering does not completely depolarize the laser light, which also was observed for example for corn fields by Kalshoven et al. (1995) and for clover by Woessner and Hapke (1987). Differences in the amount of depolarization could not be correlated to the surface type on the basis of the available data.

## 8 Simulation of a satellite instrument

One of the main goals of this study was to use the obtained lidar ground reflectance data to derive the retrieval error that would be introduced in a spaceborne IPDA measurement by an imperfect online/offline-overlap using the example of A-SCOPE. The configuration parameters used are summarized in Table 4.

The A-SCOPE laser footprint is assumed to have a gaussian beam intensity distribution, with a full width half maximum of 38 m on ground. More than 99% of the incident energy is enclosed in a circular footprint with a diameter of 100 m on ground. To upscale the reflectivity data to this footprint, the 1-D unweighted upscaling method is used with an averaging interval of 100 m length. As already mentioned, this method is very simple to implement and gives an estimate of the real 2-D gaussian averaging.

The A-SCOPE instrument will average the obtained data over a 50 km path length to decrease the statistical noise. Due to the 50-Hz laser double pulse repetition rate, a number of about 350 averaged measurements results. To account for this measurement strategy, the calculation of the retrieval error generated by an imperfect overlap using the TROPOLEX data is also based on 350 measurements selected from 50-km ground track intervals, using the same spatial sampling as for A-SCOPE. The simulation principle is described by Fig. 14. The analogy to the conditions of A-SCOPE measurements

**Table 4.** A-SCOPE configuration parameters assumed for the retrieval error simulation.

Parameter	value
Platform altitude	$\approx 400$ km
Platform speed projected on ground	$\approx 7$ km/s
Laser pulse operation	50 Hz double pulses
On/off time separation	250 $\mu\text{s}$
Averaging interval	50 km
Averaged pulse pairs	350
Laser footprint	gaussian, 38 m FWHM
Assumed spatial on-off mismatch (worst case)	10 m
CO <sub>2</sub> total column optical depth	$\Delta\tau=1$
CO <sub>2</sub> column mixing ratio	380 ppm

gives a realistic impression about the distribution of occurring retrieval errors from real ground tracks. It emerged, that the retrieval error of a single 50-km interval depends strongly on the effectively selected data, so it depends strongly on the starting point within the interval. The whole dataset collected during this project contains 38 of such 50-km intervals from different regions across Europe (land surfaces), each providing a continuous ground track data stream without interruptions.

The retrieval error of the carbon dioxide column mixing ratio for a single 50-km-interval is calculated on the basis of the Eqs. (4), (5) and (6):

$$\delta X_{\text{CO}_2} = \frac{1}{2 \Delta\tau_{\text{CO}_2}} \left[ \frac{\delta\rho}{\rho} \right]_{50\text{km}} \cdot X_{\text{CO}_2} \quad (30)$$

with  $[\delta\rho/\rho]_{50\text{km}}$  as the arithmetic mean of the 350 selected 1-D upscaled ( $\delta\rho/\rho$ )-values along the 50-km track section (100 m footprint, i.e.  $n = 11$ , see Eq. 6),  $\Delta\tau_{\text{CO}_2}$  as the differential optical depth of the CO<sub>2</sub> column and  $X_{\text{CO}_2}$  as the column mixing ratio of carbon dioxide. For the calculation of  $\delta\rho/\rho$  the original shift of about 10 m of the TROPOLEX data is taken. Hence, no further inter- or extrapolations of the collected data are done for the calculation of the resulting retrieval error. The expected online/offline overlap mismatch of a spaceborne system, such as A-SCOPE, is in the order of a few meters. So, 10 m is a conservative approach. The dominant contributor is the laser pointing jitter that can lead to shifts on ground up to 1/10 of the ground spot diameter (as a worst case). The second factor is the platform velocity that causes a shift of about 1.5 m on ground assuming the A-SCOPE configuration. A minor reason is given by the satellite platform jitter due to micro-vibrations that can not be corrected by the attitude and orbit control systems (AOCS) of a satellite, which could cause a shift of about 0.5 m (ESA, 2008).

However, the 50-Hz-pattern disregards many TROPOLEX data between consecutive A-SCOPE measurements: data are taken every 144 m, i.e. every 16 TROPOLEX measurements. To fully utilize the available dataset and to consider the dependence on the starting point, the pattern is shifted 15 times

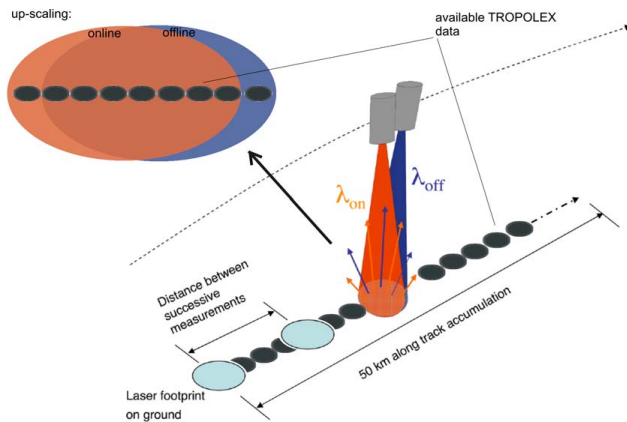


**Fig. 14.** Illustration of the A-SCOPE retrieval error calculation using TROPOLEX ground reflectance data.

within each 50-km-interval, each by one TROPOLEX measurement. The original measurements are used several times by this procedure, but the high spread of the results legitimates the use as independent values. So there is an ensemble of 16 retrieval error values for each 50-km-interval, which could be interpreted as 16 different satellite overflights along the same ground track.

Figure 15 shows a histogram of all calculated  $[\delta\rho/\rho]_{50\text{km}}$  in percent and the resulting retrieval errors in ppm (38 times 16 values are represented).

The RMS of all these single results is:  $\text{RMS}[\delta\rho/\rho]_{50\text{km}}=0.11\%$  corresponding to  $\delta X\text{CO}_2=0.22$  ppm. It has to be reminded, that these numbers base on conservative assumptions (1-D-upscaling procedure and large online/offline-mismatch) and so they are upper bounds. The retrieval error resulting for sea surfaces is below 0.1 ppm (calculated on the basis of Eq. 27).

The precision requirements defined for A-SCOPE are below 1 ppm (ESA, 2008). So it results, that the contribution of the retrieval errors, introduced by the earth's surface reflectance variability, to the total instrument error budget is not negligible, but still in an acceptable range. Inversely, the requirements that have to be satisfied by the satellite system with respect to the online/offline ground spot overlap mismatch turn out to be around 10 m or below.

## 9 Summary and outlook

The IPDA lidar technique is a promising approach for measuring atmospheric  $\text{CO}_2$ , and has been proposed for the A-SCOPE ESA mission. The purpose of this study was to investigate the impact of ground lidar reflectivity variations which are creating radiometric errors specific to IPDA lidar systems. To do so, airborne measurements of the lidar ground reflectivity at 1.57  $\mu\text{m}$  were performed with a high spatial resolution of about 10 m. The measurement flights

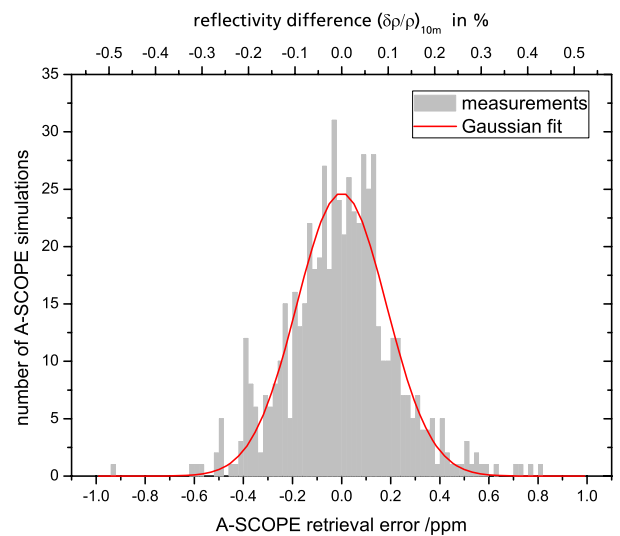


**Fig. 15.** Histogram for A-SCOPE retrieval errors (bin size: 0.02 ppm) and corresponding relative reflectance differences on the basis of all data collected during this project.

performed cover regions in Central and Western Europe with typical terrains, both in semi-arid und humid regions: primarily agricultural land, forests, populated areas, mountainous regions and the open sea. Differential absorption lidars that use the ground reflex of a laser pulse are affected by the variability of the ground surface, if adjacent online and offline pulses hit different areas on ground. Due to the laser pointing jitter and the platform velocity of a spaceborne system, a difference in the geometrical overlap of the temporally separated online and offline measurements up to 10 m has to be expected.

The performed measurements showed, that the ground surface reflectivity is highly variable in the considered spectral region. On a spatial scale of 10 m large reflectivity differences in the order of several tens of percent (RMS) occur from footprint to footprint, if the footprint diameter is also about 10 m. However, if larger footprints are of interest the reflectivity differences decrease noticeably. Conceivable satellite systems would have a laser footprint on ground with several tens of meters in diameter. Different approaches of upscaling the available data to larger footprints are investigated including a comparison to 2-D data, that are obtained by a special flight pattern. It results, that a simple 1-D averaging along a certain ground track interval leads to an acceptable approximation of a 2-D footprint with gaussian shape having a corresponding diameter. One characteristic of the reflectivity differences is their symmetrical distribution with respect to zero, which is expected due to the isotropy of the surface structures. Relevant is the number of measurements that have to be averaged to get acceptable values. Calculations using the available data showed, that for an assumed 100-m footprint diameter the averaging over 350 measurements along the track leads to a reduction of the reflectivity

differences per 10 m to below 0.11%, which corresponds to a retrieval error of below 0.22 ppm (CO<sub>2</sub> column mixing ratio). This is compatible with a spaceborne IPDA error budget, such as assumed for A-SCOPE.

Furthermore, the collected data are compared to MODIS ground reflectance data to get access to absolute values. As a first approach of an absolute calibration the MODIS data were connected directly to our data. On that basis the minimum and maximum absolute reflectances found in the collected dataset correspond to snow covered grassland with  $\rho^*=0.012\text{ sr}^{-1}$  and dry grass occurring in Southern Spain with  $\rho^*=0.18\text{ sr}^{-1}$ . By means of the MODIS land surface data also access to the sea surface reflectance was given. For wind speeds between 2 and 5 m/s we deduced a reflectance between 0.02  $\text{sr}^{-1}$  and 0.05  $\text{sr}^{-1}$ . However, according to Cox and Munk values between 0.045  $\text{sr}^{-1}$  and 0.125  $\text{sr}^{-1}$  were expected for the observed cases. This under-estimation of the lidar ground reflectance, if MODIS data are directly used for a calibration, can be explained by the hotspot effect that is occurring for the lidar measurement geometry.

Some ground types that occur on Earth's surface are not captured in the framework of this project. Future measurements should focus on further ground types that cover large areas of the Earth, such as deserts, large snow covered areas with different snow types (Larsson et al., 2006), other types of forests (e.g. in the tropics), savannas, marshlands, tundra and sea surfaces under high wind speed conditions. Another issue that could have an impact on the surface reflectance is the surface humidity due to dew or just after rainfall (Twomey et al., 1986). In summary, the TROPOLEX system onboard the Cessna Caravan aircraft turned out to be an excellent tool to investigate the ground surface variability.

*Acknowledgements.* This project was funded by the European Space Agency (ESA) within the framework of the assessment studies for A-SCOPE, a proposed Earth Explorer Core Mission. We would like to express special thanks to the DLR Flight Facilities for supporting and conducting the flight missions as well as H. Krafczyk, R. Simmet and G. Simmet for their technical support. Additionally we thank EADS/ASTRIUM for the management of this project.

Edited by: M. Riese

## References

- Amediek, A., Fix, A., Wirth, M., and Ehret, G.: Development of an OPO system at 1.57  $\mu\text{m}$  for integrated path DIAL measurement of atmospheric carbon dioxide, *Appl. Phys. B Lasers Opt.*, 92, 295–302, 2008.
- Baldrige, A. M., Hook, S. J., Grove, C. I., and Rivera, G.: The ASTER spectral library version 2.0, *Remote Sens. Environ.*, 113(4), 711–715, 2009.
- Bréon, F. M. and Henriot, N.: Spaceborne observations of ocean glint reflectance and modeling of wave slope distributions, *J. Geophys. Res.*, 111, C06005, doi:10.1029/2005JC003343, 2006.
- Bréon, F. M., Maignan, F., Leroy, M., and Grant, I.: Analysis of hot spot directional signatures measured from space, *J. Geophys. Res.*, 107(16), 4282–4296, 2002.
- Bufton, J. L., Hoge, F. E., and Swift, R. N.: Airborne measurements of laser backscatter from the ocean surface, *Appl. Optics*, 22(17), 2603–2618, 1983.
- Camacho-de Coca, F., Bréon, F. M., Leroy, M., and Garcia-Haro, F. J.: Airborne measurement of hot spot reflectance signatures, *Remote Sens. Environ.*, 90(1), 63–75, 2004.
- Cox, C. and Munk, W.: Measurement of the roughness of the sea surface from photographs of the Sun's glitter, *J. Opt. Soc. Am.*, 44(11), 838–850, 1954.
- Disney, M. I., Lewis, P. E., Bouvet, M., Prieto-Blanco, A., and Hancock, S.: Quantifying Surface Reflectivity for Spaceborne Lidar via Two Independent Methods, *IEEE T. Geosci. Remote*, 47(9), 3262–3271, 2009.
- Ehret, G. and Kiemle, C.: Requirements Definition for Future DIAL Instruments, Final Report, ESA Study 10880/03/NL/FF, 2005.
- Ehret, G., Amediek, A., Kiemle, C., Wirth, M., Fix, A., Houweling, S., and Behrendt, A.: Spaceborne Remote Sensing of the Greenhouse Gases CO<sub>2</sub>, CH<sub>4</sub>, N<sub>2</sub>O by Path Integrated Differential Absorption Lidar: A Sensitivity Analysis, *Appl. Phys. B: Lasers Opt.*, 90, 593–608, 2008.
- European Space Agency (ESA): A-SCOPE - Advanced Space Carbon and Climate Observation of Planet Earth, Report For Assessment, ESA-SP1313/1, 2008.
- Friedman, D.: Infrared Characteristics of Ocean Water (1.5–15  $\mu\text{m}$ ), *Appl. Optics*, 8, 2073–2078, 1969.
- Giordmaine, J. A. and Miller, R. C.: Tunable Coherent Parametric Oscillation in LiNbO<sub>3</sub> at Optical Frequencies, *Phys. Rev. Lett.* 14(24), 973–976, 1965.
- Hapke, B., DiMucci, D., Nelson, R., and Smythe, W.: The Cause of the Hot Spot in Vegetation Canopies and Soils: Shadow-Hiding Versus Coherent Backscatter, *Remote Sens. Environ.*, 58, 63–68, 1996.
- Justice, C. O., Townshend, J. R. G., Vermote, E. F., Masuoka, E., Wolfe, R. E., El Saleous, N., Roy, D. P., and Morisette, J. T.: An overview of MODIS Land data processing and product status, *Remote Sens. Environ.*, 83, 3–15, 2002.
- Kaasalainen, S., Kaasalainen, M., Mielonen, T., Suomalainen, J., Peltoniemi, J. I., and Näränen, J.: Optical properties of snow in backscatter, *J. Glaciol.*, 52(179), 574–584, 2006.
- Kaasalainen, S. and Rautiainen, M.: Hot spot reflectance signatures of common boreal lichens, *J. Geophys. Res.*, 110, D20102, doi:10.1029/2005JD005834, 2005.
- Kalshoven Jr., J. E., Tierney Jr., M. R., Daughtry, C. S. T., and McMurtrey III, J. E.: Remote sensing of crop parameters with a polarized, frequency-doubled Nd:YAG laser, *Appl. Optics*, 34, 2745–2749, 1995.
- Lancaster, R. S., Spinhirne, J. D., and Palm, S. P.: Laser pulse reflectance of the ocean surface from the GLAS satellite lidar, *Geophys. Res. Lett.*, 32, L22S10, doi:10.1029/2005GL023732, 2005.
- Larsson, H., Steinvall, O., Chevalier, T., and Gustafsson, F.: Characterizing laser radar snow reflection for the wavelengths 0.9 and 1.5  $\mu\text{m}$ , *Opt. Eng.*, 45, 116201-1–116201-11, 2006.
- Liang, S. L., Fang, H. L., Chen, M. Z., Shuey, C. J., Walthall, C., Daughtry, C., Morisette, J., Schaaf, C., and Strahler, A.: Validating MODIS land surface reflectance and albedo products: meth-

- ods and preliminary results, *Remote Sens. Environ.*, 83, 149–162, 2002.
- Meister, A., Fix, A., Flentje, H., Wirth, M., and Ehret, G.: TropOLEX: A New Tuneable Airborne Lidar System for the Measurement of Tropospheric Ozone, 6th International Symposium on Tropospheric Profiling, Leipzig, Germany, 14–20 September 2003, 233–235, 2003.
- Menzies, R. T., Tratt, D. M., and Hunt, W. H.: Lidar In-space Technology Experiment measurements of sea surface directional reflectance and the link to surface wind speed, *Appl. Optics*, 37(24), 5550–5559, 1998.
- Tang, C. L., Bosenberg, W. R., Ukachi, T., Lane, R. J., and Cheng, L. K.: Optical parametric oscillators, *IEEE, Proceedings*, 80(3), 365–374, 1992.
- Twomey, S. A., Bohren, C. F., and Mergenthaler, J. L.: Reflectance and albedo differences between wet and dry surfaces, *Appl. Optics*, 25, 431–437, 1986.
- Woessner, P. and Hapke, B.: Polarization of Light Scattered by Clover, *Remote Sens. Environ.*, 21, 243–261, 1987.